Functional transcranial brain imaging by optical-resolution photoacoustic microscopy

Song Hu, Konstantin Maslov, Vassiliy Tsytsarev, and Lihong V. Wang
Washington University in St. Louis, Department of Biomedical Engineering, Optical Imaging Laboratory, One Brookings Drive, St. Louis, Missouri 63130-4899

Abstract. Optical-resolution photoacoustic microscopy (OR-PAM) is applied to functional brain imaging in living mice. A near-diffraction-limited bright-field optical illumination is employed to achieve micrometer lateral resolution, and a dual-wavelength measurement is utilized to extract the blood oxygenation information. The variation in hemoglobin oxygen saturation (sO_2) along vascular branching has been imaged in a precapillary arteriolar tree and a postcapillary venular tree, respectively. To the best of our knowledge, this is the first report on *in vivo* volumetric imaging of brain microvascular morphology and oxygenation down to single capillaries through intact mouse skulls. It is anticipated that: (*i*) chronic imaging enabled by this minimally invasive procedure will advance the study of cortical plasticity and neurological diseases; (*ii*) revealing the neuroactivity-dependent changes in hemoglobin concentration and oxygenation will facilitate the understanding of neurovascular coupling at the capillary level; and (*iii*) combining functional OR-PAM and high-resolution blood flowmetry will have the potential to explore cellular pathways of brain energy metabolism. © *2009 Society of Photo-Optical Instrumentation Engineers.* [DOI: 10.1117/1.3194136]

Advances in brain imaging facilitate the understanding of cognitive phenomena and neurological diseases. However, high-resolution brain imaging through intact animal skulls remains challenging for pure optical modalities because the optical scattering and absorption of the skull degrade the imaging resolution and signal-to-noise ratio (SNR). Photoacoustic imaging, combining light and ultrasound in a single hybrid technology, suggests a potential solution. Using acoustic-resolution photoacoustic microscopy (AR-PAM), Stein et al. recently demonstrated mouse brain imaging through both intact scalp and skull.[1] This noninvasive feature is highly desirable for functional or chronic studies; however, with its current spatial resolution (lateral resolution: 70 μm; axial resolution: 54 μm), capillaries are not resolvable. To fill the

Address all correspondence to: Lihong V. Wang, Tel: (314) 935-6152; Fax: (314) 935-7448; E-mail: lhwang@biomed.wustl.edu
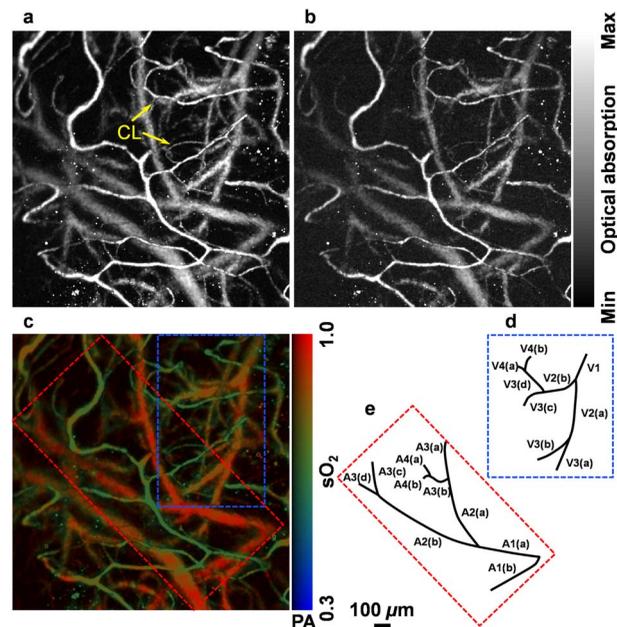
Fig. 1 *In vivo* functional OR-PAM imaging of mouse brain microvasculature through an intact skull. (a) MAP image acquired at 570 nm; (b) MAP image acquired at 578 nm; (c) vessel-by-vessel sO_2 mapping; (d) a venular tree with branching orders [boxed by blue dashed lines in (c)]; (e) an arteriolar tree with branching orders [boxed by red dashed lines in (c)]. The calculated sO_2 values are shown in the color bar. PA: photoacoustic signal amplitude. The scale bar applies to (a), (b), and (c). (Color online only.)

gap, Maslov et al. developed optical-resolution photoacoustic microscopy (OR-PAM) capable of imaging single capillaries *in vivo*.[2] The lateral resolution of OR-PAM matches the size of a single red blood cell (RBC), and its sensitivity enables single RBC detection.[3]

Here, we report on the first demonstration of OR-PAM for functional brain microvascular imaging down to single capillaries through intact mouse skulls. The minimally invasive feature is favorable for chronic study of cortical plasticity. Moreover, because neuronal activity is widely assumed to spatially correlate most closely to the capillary bed response,[4] improving localization of signals down to the capillary level will enable functional brain mapping at micrometer resolution.

Before functional brain imaging, a Swiss Webster mouse (Hsd:ND4, Harlan Co., 25 – 30 g) was anesthetized by intraperitoneally administering a dose of 87 mg/kg ketamine and 13 mg/kg xylazine and transferred to a stereotaxic imaging stage. The scalp of the mouse was surgically removed, and the exposed skull was cleaned with 0.9% sodium chloride irrigation solution right before imaging. Ultrasonic gel was used for ultrasound coupling and maintaining skull hydration. Throughout the experiment, the animal was supplied with breathing-grade air and maintained under anesthesia using vaporized isoflurane (1.0–1.5% isoflurane with an airflow rate of 1 L/min). The body temperature of the animal was maintained at 37 °C by a temperature-controlled heating pad. At the end of the experiment protocol, the animal was euthanatized by an intraperitoneal administration of pentobarbital at a
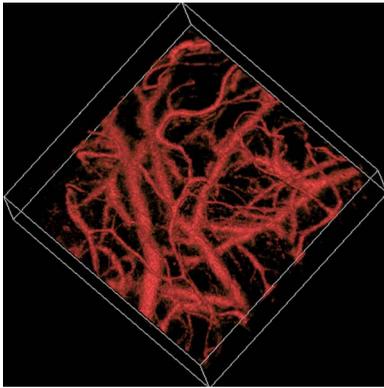
Video 1. *In vivo* volumetric visualization of the mouse brain microvasculature through an intact skull by OR-PAM (QuickTime 4 MB) [URL: http://dx.doi.org/10.1117/1.3194136.1].

dosage of 100 mg/kg. The detailed system description can be found in our published papers.[2,3]

In photoacoustic measurements of hemoglobin concentration and oxygenation, we assume that, in the visible spectral range, oxyhemoglobin (HbO_2) and deoxyhemoglobin (HbR) are the dominant absorbing compounds in blood.[5] Thus, a dual-wavelength measurement is adequate to image sO_2, though using more wavelengths is expected to yield more accurate results.[6] The two wavelengths chosen here are 570 and 578 nm, where the absorption contrast between blood and background brain tissues are high enough to enable satisfactory imaging quality.[5] According to the published absorption spectra of rat hemoglobin,[7] 570 nm is an isosbestic point, at which HbO_2 and HbR have the same molar extinction coefficients. Thus, the photoacoustic signal acquired at this wavelength reflects the total hemoglobin concentration (HbT), and 578 nm is an HbO_2-absorption-dominant wavelength, which helps differentiate the two types of hemoglobin. Because blood oxygenation is highly correlated with local metabolism, the sO_2 value is generally time variant. To minimize measurement error due to the possible temporal fluctuation in blood

oxygenation, we implemented a wavelength autotuning program to control the dye laser, and imaged the same cross-sectional scan (B-scan) for each of the wavelengths before moving to the next B-scan. The region of interest (ROI) was scanned with a step size of 2.5 μm. The dual-wavelength measurement took ~20 min, which was mostly limited by the wavelength tuning speed of the dye laser.

Figures 1(a) and 1(b) are maximum amplitude projection (MAP) images of the mouse brain microvasculature under systemic normoxia at the optical wavelengths of 570 and 578 nm, respectively. Because 570 nm is an isosbestic point, Fig. 1(a) maps the HbT, regardless of the blood oxygenation. Microvessels labeled with CL in Fig. 1(a) appear to be single capillaries with diameters of 5–10 μm. A corresponding volumetric rendering is shown in Video 1. At the conclusion of the dual-wavelength measurement, the concentrations of HbR and HbO_2, as well as the sO_2 values, were calculated based on the model described in previously published work.[5,6] As shown in Fig. 1(c), different sO_2 levels are visualized with pseudocolors ranging from blue to red, while the HbT measured at the isosbestic point (570 nm) is represented by pixel brightness. According to known physiology, the red vessels (sO_2 values of >90%) are believed to be arterioles, whereas the green ones (sO_2 values as low as 60–70%) are most likely to be venules. However, in the microcirculation, there is no clear cutoff in sO_2 value between arterioles and venules.[8] The blood oxygenation is closely associated with the microvascular branching order[8] and the local metabolic activity of the tissue.[9] To demonstrate the oxygen gradients in the brain microcirculation, we selectively analyzed a postcapillary venular tree [Fig. 1(d)] and a precapillary arteriolar tree [Fig. 1(e)] highlighted in Fig. 1(c) by the blue and red dashed boxes, respectively. The vessel diameters and the corresponding sO_2 values in different branching orders are listed in Tables 1 and 2. A negative correlation between the branching order and its mean sO_2 value is observed in both the arteriolar and venular trees with a linear regression analysis (arteriolar tree: R^2 =0.98, p=0.01; venular tree: R^2=0.75, p=0.14), as shown in

Table 1 The vessel diameters and the sO_2 values in different branching orders in a venular tree. Values are in mean±standard deviation format.

Branching order	1	2		3				4	
Vessel ID	V1	V2(a)	V2(b)	V3(a)	V3(b)	V3(c)	V3(d)	V4(a)	V4(b)
Diameter (μm)	57±2	48±5	42±3	35±2	30±2	41±2	24±3	20±2	19±3
sO_2 (%)	83±3	83±3	85±2	86±3	83±3	78±2	75±4	74±5	76±4

Table 2 The vessel diameters and the sO_2 values in different branching orders in an arteriolar tree. Values are in mean±standard deviation format.

Branching order	1		2		3				4	
Vessel ID	A1(a)	A1(b)	A2(a)	A2(b)	A3(a)	A3(b)	A3(c)	A3(d)	A4(a)	A4(b)
Diameter (μm)	59±4	48±3	43±4	52±2	44±4	32±2	51±2	42±4	23±3	24±2
sO_2 (%)	93±2	93±2	91±3	91±3	89±2	88±4	87±3	79±3	85±2	81±3
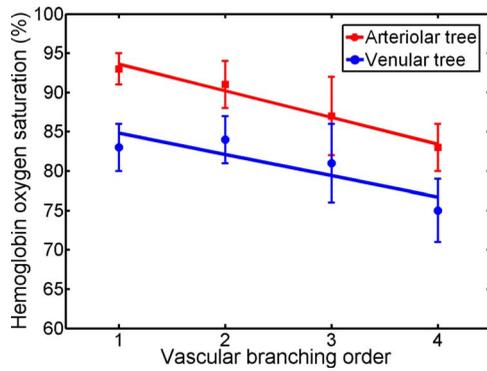
Fig. 2 The sO$_2$ value versus the vascular branching order in a precapillary arteriolar tree and a postcapillary venular tree. The square and round markers represent the mean sO$_2$ values in each branching order, and the error bars stand for the standard deviations of the mean sO$_2$ values.

Fig. 2. Our results suggest that: (*i*) the blood oxygenation level is higher in the arteriolar tree than in the venular tree; (*ii*) capillaries are not the only oxygen exchange site in the microcirculation because the sO$_2$ decreases significantly with vascular branching in the precapillary arteriolar tree ($\sim$12% from order 1 to 4); and (*iii*) a diffusional shunt is present between arterioles and venules to elevate the oxygen level in "large" venules because the sO$_2$ increases noticeably with blood confluence in the postcapillary venular tree ($\sim$9% from order 1 to 4). Our observation is in agreement with the published work.[8–10]

According to a previous study,[11] the wavelength-dependent optical attenuation due to the intact skull affects the measurement accuracy. Here, this wavelength dependence was estimated by measuring the photoacoustic signals of a black polyethylene film attached beneath the skull of a freshly sacrificed mouse of the same type at the two operating wavelengths, respectively. The mouse skull was submerged in 0.9% sodium chloride irrigation solution to keep hydration. Because the black polyethylene film can be considered as a neutral absorber in the visible spectral range, the wavelength dependence in the photoacoustic signals is expected to be predominantly from the mouse skull. If we consider the skull to be homogeneous within the ROI,[5] then such dependence can be simply compensated for by applying different calibration factors to the measured photoacoustic signals at different optical wavelengths. However, the wavelength-dependent optical scattering and absorption of brain tissues are difficult to compensate for due to heterogeneous tissue structure and composition.

In summary, OR-PAM has been applied to mouse brain imaging through intact skulls with capillary-level spatial resolution. Functional information of HbT and sO$_2$ within single microvessels was imaged simultaneously using a dual-wavelength measurement. The ability to extract brain oxygen saturation information on a single-capillary basis with minimal invasiveness makes OR-PAM a potential tool for high-resolution functional brain mapping, quantitative analysis of brain energy metabolism, and chronic studies of cortical plasticity and neurological diseases. It is worth noting that the maximum imaging depth of OR-PAM, estimated from the surface of the intact skull, is 500–600 μm when the system is operated at the Q-band of the hemoglobin absorption spectrum (optical wavelength: $\sim$560 nm). This penetration is slightly less than the typical imaging depth of two-photon microscopy (TPM) (600–800 μm) through a skull window with near-infrared (NIR) excitation,[12] where no bone is in the optical path. NIR light sustains less brain tissue absorption and scattering than visible light. However, owing to the quadratic intensity dependence in two-photon generation and linear dependence in OR-PAM, the light scattering and absorption within the intact skull as well as the surface scattering at the skull-brain interface decreases the fluorescence signal in TPM much faster than the photoacoustic signal in OR-PAM. As a result, TPM has not demonstrated transcranial imaging. By utilizing NIR operation and compromising the lateral resolution, doppler optical coherence tomography can extend the imaging depth to $\sim$1.5 mm.[13] To enhance the penetration of OR-PAM, system SNR or imaging contrast needs to be further improved.

References

1. E. W. Stein, K. Maslov, and L. V. Wang, "Noninvasive, *in vivo* imaging of blood-oxygenation dynamics within the mouse brain using photoacoustic microscopy," *J. Biomed. Opt.* **14**(2), 020502 (2009).
2. K. Maslov, H. F. Zhang, S. Hu, and L. V. Wang, "Optical-resolution photoacoustic microscopy for *in vivo* imaging of single capillaries," *Opt. Lett.* **33**(9), 929–931 (2008).
3. K. Maslov, H. F. Zhang, S. Hu, and L. V. Wang, "Optical-resolution confocal photoacoustic microscopy," *Proc. SPIE* **6856**, 68561I (2008).
4. E. M. Hillman, A. Devor, M. B. Bouchard, A. K. Dunn, G. W. Krauss, J. Skoch, B. J. Bacskai, A. M. Dale, and D. A. Boas, "Depth-resolved optical imaging and microscopy of vascular compartment dynamics during somatosensory stimulation," *Neuroimage* **35**(1), 89–104 (2007).
5. X. Wang, X. Xie, G. Ku, L. V. Wang, and G. Stoica, "Noninvasive imaging of hemoglobin concentration and oxygenation in the rat brain using high-resolution photoacoustic tomography," *J. Biomed. Opt.* **11**(2), 024015 (2006).
6. H. F. Zhang, K. Maslov, M. Sivaramakrishnan, G. Stoica, and L. V. Wang, "Imaging of hemoglobin oxygen saturation variations in single vessels *in vivo* using photoacoustic microscopy," *Appl. Phys. Lett.* **90**(5), 053901-1-053901-3 (2007).
7. W. G. Zijlstra, A. Buursma, and O. W. van Assendelft, *Visible and Near Infrared Absorption Spectra of Human and Animal Hemoglobin, Determination and Application*, VSP, Amsterdam, The Netherlands (2000).
8. H. Kobayashi and N. Takizawa, "Oxygen saturation and pH changes in cremaster microvessels of the rat," *Am. J. Physiol.* **270**(4), H1453–1461 (1996).
9. A. G. Tsai, P. C. Johnson, and M. Intaglietta, "Oxygen gradients in the microcirculation," *Physiol. Rev.* **83**(3), 933–963 (2003).
10. E. Vovenko, "Distribution of oxygen tension on the surface of arterioles, capillaries and venules of brain cortex and in tissue in normoxia: an experimental study on rats," *Pfluegers Arch.* **437**(4), 617–623 (1999).
11. X. Wang, D. L. Chamberland, and G. Xi, "Noninvasive reflection mode photoacoustic imaging through infant skull toward imaging of neonatal brains," *J. Neurosci. Methods* **168**(2), 412–421 (2008).
12. F. Helmchen and W. Denk, "Deep tissue two-photon microscopy," *Nat. Methods* **2**(12), 932–940 (2005).
13. R. K. Wang, S. L. Jacques, Z. Ma, S. Hurst, S. R. Hanson, and A. Gruber, "Three dimensional optical angiography," *Opt. Express* **15**(7), 4083–4097 (2007).